



Characteristic Changes in the Strengthening Western Disturbances over Karakoram in Recent Decades

Aaquib Javed¹ · Pankaj Kumar¹

Received: 6 June 2023 / Revised: 4 February 2024 / Accepted: 5 February 2024 / Published online: 14 February 2024
© The Author(s) under exclusive licence to Korean Meteorological Society and Springer Nature B.V. 2024

Abstract

Western disturbances (WDs) are upper-tropospheric mid-latitude synoptic systems propagating eastward along the subtropical westerly jet stream. They are capable of causing extreme precipitation events and have strengthened their impact over the Karakoram part of the Himalayas in recent decades. They play a crucial role in the sustenance of the “Karakoram Anomaly,” which refers to the anomalous stability/surge of a few Karakoram glaciers in contrast to the other glaciers of the Himalayas. Using the existing WD-catalog derived from ERA5 and MERRA2 reanalysis datasets, we observed that the core genesis zone for Karakoram WDs had undergone a statistically significant shift of $\sim 9.7^\circ\text{E}$, migrating towards more favourable conditions for cyclogenesis. The study proposes a new parameter to identify regions of potential extratropical cyclogenesis. The shift can be attributed to an enhanced genesis potential, convergence, and higher moisture availability along the WD path. Composite analysis suggests that moisture availability has risen significantly over the shifted zone. Moreover, the propagation speeds of these systems have significantly declined, which explains the recent intensification of precipitation events related to WDs over the Karakoram and hints toward a crucial synoptic influence on the anomalous regional mass-balance phenomenon.

Keywords Western disturbances · Karakoram anomaly · Climate change · Tracking algorithm

1 Introduction

The precipitation over Karakoram-Himalayas (KH) during boreal winter primarily comes from the mid-latitude synoptic systems called Western disturbances (WDs), traveling eastward embedded in the subtropical westerly jet stream (Dimri et al. 2015; Hunt et al. 2018b). They form an integral part of the regional winter climate, critical in establishing and sustaining the regional snowpack and water resources (Dimri et al. 2015). About two-thirds of the winter snowfall over KH is received through WDs, profoundly impacting the glaciers of the largest ice mass outside the poles (Bashir et al. 2017; Bolch et al. 2012; Javed et al. 2022). The snowfall influx provided by WDs during the accumulation period plays a crucial role in modulating the regional mass-balance estimations (Farinotti et al. 2020; Kumar et al. 2019; Mölg et al. 2014; Nie et al. 2021). The glaciers of the KH have

mainly receded in recent decades (Romshoo et al. 2020, 2022), much like other glacial regions of the world. However, the Karakoram (KR) region of KH has exhibited an exceptional divergent response, showing anomalous stability/surge in some of its glaciers. This phenomenon is known as the “Karakoram Anomaly” (Kumar et al. 2015; Quincey et al. 2011). Several hypotheses explaining the probable triggers and underlying mechanisms behind the phenomenon have been speculated since (de Kok et al. 2018; Dimri 2021; Farinotti et al. 2020; Forsythe et al. 2017; Kapnick et al. 2014; Vishwakarma et al. 2022).

Stable glacier mass budgets in Central Karakoram were initially noticed after observing a decline in river flow since 1961 (Gardelle et al. 2012). However, the theory was later challenged when an increasing trend in river flow was established between 1985 and 2010 (Mukhopadhyay and Khan 2014). The complex interaction of the monsoon and mid-latitude westerlies during summer gives rise to intricate patterns of interannual precipitation variability (Kapnick et al. 2014). It has been linked to the Karakoram/Western Tibetan Vortex, which is an atmospheric feature identified using a regional circulation metric that quantifies the relative position and intensity of the westerly jet (Forsythe et al.

✉ Pankaj Kumar
kumarp@iiserb.ac.in

¹ Department of Earth and Environmental Sciences, Indian Institute of Science Education and Research Bhopal, Bhopal By-Pass Road, Bhauri, Bhopal 462066, India

2017; Li et al. 2018). Evidence from weather stations and tree rings suggests an augmentation of diurnal temperature ranges during the latter half of the twentieth century (Yadav et al. 2004). Cooler summers have been proposed as a crucial factor influencing the overall equilibrium of the Karakoram glacier budget in the past few decades (Fowler and Archer 2006; Kapnick et al. 2014). Some studies have attributed increased glacial surge to enhanced evaporation due to intense irrigation activities after 1960. The heightened atmospheric moisture levels led to an increased cloud cover and a decrease in incoming shortwave radiation, thereby diminishing ice and snow ablation during summers (de Kok et al. 2018). The anomaly is mainly concentrated in the Central Karakoram and cease to exist as we approach the eastern edge of Karakoram (Negi et al. 2021).

However, apparent shortcomings persist, such as WDs' role in modulating regional hydrology and glacial anomaly (Cannon et al. 2016; Norris et al. 2015, 2017, 2018). Most studies exploring the phenomenon are hampered by the lack of observational datasets for the region (Figure-1a, inset), primarily because of being altitudinally inaccessible and its extreme topography (Azam et al. 2021; Brun et al. 2017). Dimri et al. 2015 synthesized past research on WDs and suggested the need for a comprehensive assessment of the state of knowledge. A previous study has explored the large-scale dynamics of WDs using a tracking algorithm applied to the upper-tropospheric vorticity field for 37 years of European Centre for Medium-Range Weather Forecasts (ECMWF) Re-Analysis Interim (ERA-Interim) data, giving a catalog of over 3000 events (Hunt et al. 2018b). The study analyzed the vertical structure of WDs in a composite framework, exploring many dynamic and thermodynamic fields. Another study addressed WD dynamics using a wave-tracking algorithm based on 500 hPa geopotential height anomaly and identified a relationship between the strength of disturbances and the state of the background environment during their propagation (Cannon et al. 2016). Another study have observed a decline in WD activity over Northern India during boreal winters in recent decades, resulting in a reduced precipitation contribution in the region except for highest altitudinal stretches of Himalayas (Javed et al. 2023). Although WDs can be present at any given time of the year, their occurrence peaks during the winter bringing in a considerable amount of snowfall, the most crucial parameter for glacier mass-budget estimation during the accumulation period (Kumar et al. 2019). It has also been reported that North Atlantic Oscillation significantly affects WD behaviour on interannual timescales over Western Himalayas (Hunt and Zaz 2022).

The requirement is to quantify the extent of their role in characterizing the regional anomaly. A predecessor of the present study (Javed et al. 2022) establishes WD-associated winter precipitation as one of the key drivers behind the emergence of the anomaly. Using a tracking algorithm applied to 39-seasons

(1980–2019; November–March) of vorticity at 300 hPa and 400 hPa levels for three different reanalysis datasets, the associated reanalysis ensemble statistics of WDs properties suggest a revival in recent years over the core-anomaly regions (Javed et al. 2022). The KR witnessed a rise of about ~10% in WD-associated precipitation intensity in the last two decades, coinciding with the anomaly period. Furthermore, WDs were responsible for nearly ~65% of the total seasonal snowfall, underlining their crucial role in modulating the regional mass-balance anomaly (Javed et al. 2022). The study also highlighted the ability of the tracking algorithm to produce similar synoptic signatures using different reanalysis datasets with a considerably good match among themselves. The present study uses the existing WD catalog of two reanalyses datasets from its predecessor (the two having the best match) and tries to bring forth the factors propelling the changes associated with WDs directly impacting the “Karakoram Anomaly.” The study starts with an outline of the study region (Section 2), data sources (Section 3.1–3.3) and the methodology employed (Section 3.4–3.5). The result section primarily discusses the changes associated with the shift in genesis locations of Karakoram WDs (Section 4.1). Possible mechanisms triggering the shift and their resultant impact on moisture-carrying capacity are discussed in detail in Section 4.2. We conclude the discussion in Section 5.

2 Study Region

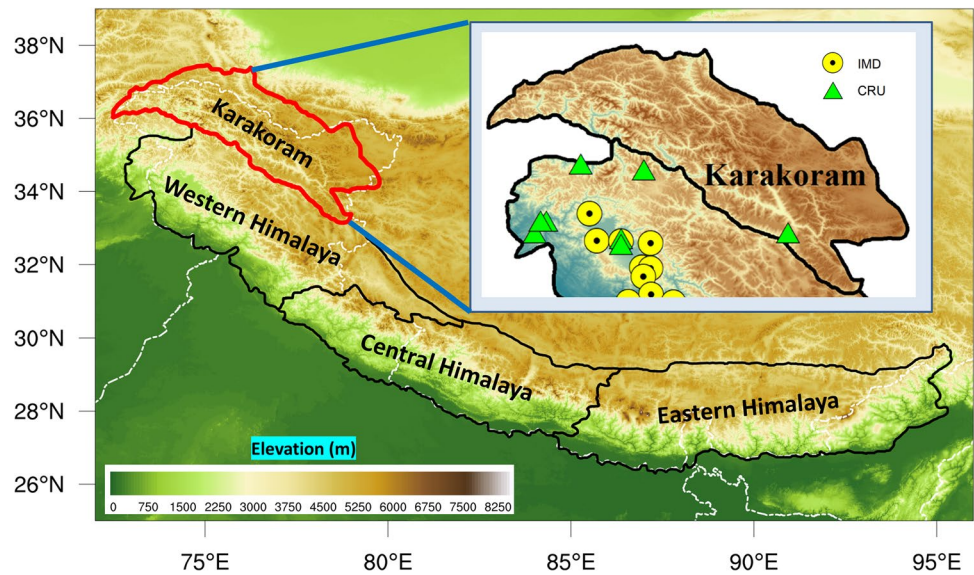
Figure 1 depicts the study region, its geographical location, mean altitude, and the apparent lack of in-situ observational stations in the Karakoram. It is the northernmost part of the KH, having the highest mean altitude and large glacierized area compared to the other regions. The region suffers from acute scarcity of observational data records, inhibiting research which are dependent on in-situ datasets. The present study extends the results of Javed et al. 2022, pivoting solely on the WDs passing through KR to focus on their impact in modulating the anomaly and investigating the plausible mechanisms behind their resurgence. Most of the studies investigating the anomalous behaviour of Karakoram glaciers focuses on the regional mechanisms and manifestations. However, the novelty of the present study lies in unravelling a crucial synoptic-level influence on a regional phenomenon and discussing possible triggers behind their characteristic changes.

3 Data and Methods

3.1 ERA5

The ERA5 reanalysis dataset (Copernicus Climate Change Service (C3S), 2017) is the latest reanalysis from the

Fig. 1 Shows the mean elevation (m) and geographical location of KR (red outline) and other KH regions (black outline). The white outline denotes Indian geopolitical territory. The zoomed-inset figure highlights the acute scarcity of in-situ observational stations in the Karakoram. Yellow circles are the Indian Meteorological Department (IMD) stations, whereas green triangles are the Climate Research Unit (CRU) land stations



ECMWF. It replaces its predecessor, ERA-Interim reanalysis (Dee et al. 2011), and has a relatively enhanced horizontal (TL639, spectral model, 31 km) and vertical resolutions (137 levels to 0.01 hPa, hybrid sigma-pressure) with an hourly temporal output. It is based on 4D-Var data assimilation with a 12-hour window and variational bias correction of observations using Cycle 41r2 of the Integrated Forecasting System (Hersbach et al. 2019). The data is freely available for the period from 1940 to the present. The data can be accessed from: <https://cds.climate.copernicus.eu/cdsapp#!/search?text=ERA5%20hourly>.

3.2 MERRA2

The Modern-Era Retrospective analysis for Research and Applications, Version 2 (MERRA-2) (Gelaro et al. 2017) is a global atmospheric reanalysis produced by the NASA Global Modeling and Assimilation Office (GMAO). It covers the satellite-observing era from 1980 to the present and is freely available. It replaces its predecessor, MERRA (Rienecker et al. 2011). MERRA2 has a horizontal resolution of $0.625^{\circ} \times 0.5^{\circ}$ and 72 hybrid-eta levels up to 0.01 hPa. Past observations are assimilated using a 3D-Variational system with a 6-hour update cycle, which only adjusts model projections forward in time. The data can be accessed from: https://gmao.gsfc.nasa.gov/reanalysis/MERRA-2/data_access.

3.3 REMO_{glacier}

The estimates of regional mass balance for KR glaciers are obtained from a high-resolution glacier-climate model called REMO_{glacier}. This model combines the atmospheric regional model REMO (Jacob and Podzun 1997) with a dynamic glacier parameterization scheme (DGS) (Kotlarski

2007; Kotlarski et al. 2010). The DGS represents the surface glacier cover at a smaller scale and calculates the energy and mass balance of the glacierized part within each grid box. The glacierized part can dynamically grow or shrink based on the simulated mass balance, but it is constrained to the total land surface area of the respective grid box. The integration of REMO_{glacier} covers the South Asian region (7° – 38° N, 65° – 98° E) from 1989 to 2016, taking into account the availability of glacier inventory for initializing the model, as used in previous studies (Frey et al. 2014; Pfeffer et al. 2014). The setup has a horizontal resolution of $0.22^{\circ} \times 0.22^{\circ}$ (approximately 25 km) with 27 vertical levels. It is forced by the ERA-Interim dataset for lateral boundary conditions, which are updated every 6 h and interpolated to a 2-minute time step (Kumar et al. 2015).

3.4 WD Track Database

The existing WD database of ERA5 and MERRA2 was taken from Javed et al. 2022, which applied the tracking algorithm called “TRACK” (Curio et al. 2019; Hodges et al. 2017; Pinheiro et al. 2019). The tracking is performed using T63 spectrally filtered relative vorticity field averaged between 400 hPa and 300 hPa levels (Hunt et al. 2018a, 2019a) at a 3-hourly temporal resolution for 39 winter seasons (1980–2019, November–March), considered the most active period for WDs (Krishnan et al. 2018). The study period (1980–2019) has been divided into two sub-periods: P1 (1980–2000) and P2 (2001–2019), based on the outcome of a change point detection method (using Pettitt’s test) applied on the amount of snowfall (and total precipitation) received by the Karakoram region. The test revealed a significant change point in 2001 at a 95% confidence level (Fig. 2). The figure depicts a reversal in trend for both

precipitation and its solid component between the two identified sub-periods. The period segregation aptly coincides with the observed glacier variability of Karakoram glaciers, previously discussed in various studies (Azam et al. 2018; Berthier and Brun 2019; Dehecq et al. 2019). By comparing and analyzing various parameters and characteristics within the two sub-periods, the study attempts to unravel the reasons behind this behavioral change of WDs impacting the KR glaciers.

The WD database includes a domain-filtering constraint, with the tracks required to pass through a KR box bounded by 33–37.5°N and 72.3–80°E, resembling the smallest rectangular domain covering the whole of KR (Fig. 3). This filters out a significant chunk of WDs which do not directly impact the glaciers of KR in terms of providing snowfall influx. The tracks were also required to breach a vorticity (intensity) threshold of $1 \times 10^{-5} \text{ s}^{-1}$ (Pinheiro et al. 2019; Priestley and Catto 2022), sustain themselves at least for a day, and travel 1000 km. A track-matching methodology was employed to select the best tracks among the two reanalysis datasets, i.e., having a good temporal and spatial match (10% points match within a 4° radius). About ~52% of ERA5 tracks were found to have a good match with MERRA2 (Javed et al. 2022). Most of the matching tracks were of higher intensities, whereas the smaller intensity storms had difficulty qualifying the matching criteria. It should be kept in mind that most of WD-associated precipitation contribution comes from higher intensity storms whereas the low intensity storms are either dry or don't last long enough to precipitate. Therefore, even if low intensity tracks are filtered out, the information loss is not significant. In totality, ERA5 could identify 484 (out of which 252 matched) WDs passing through KR, whereas MERRA2 identified 519 WDs between 1980 and 2019. Figure 3a depicts the tracks of ERA5 that matched with MERRA2 and their genesis locations, while Fig. 3b

demonstrates the mean path of WDs in the two sub-periods, P1 and P2. All WD associated statistics discussed in the present study are ensemble mean of the two reanalysis datasets to reduce the uncertainties.

3.5 Mid-Latitude Genesis Potential

Previous studies have identified a few parameters that significantly factor into the evolution of WDs. Geopotential height has been a common denominator in most of them, mainly because they are synonymous with deep troughs within and exhibit well-defined signatures (Cannon et al. 2015, 2016; Dimri and Chevuturi 2014; Lang and Barros 2004; Madhura et al. 2015). Recently, Midhuna et al. 2020 proposed a new geopotential height anomaly-based Western Disturbance Index (*WDI*) to corroborate the characteristics of WDs with their associated dynamics. The study found that *WDI* is correlated positively with the number of WDs in a season. Similarly, baroclinic instability and the location of subtropical westerly jetstream (STWJ) play a significant role in the early stages of WD development and are considered crucial factors in determining the location and frequency of their genesis (Hunt et al. 2018a, b; Javed et al. 2022). Regions of higher baroclinicity are associated with higher genesis activity. Another well-known index, generally employed to study tropical cyclogenesis (Tiwari et al. 2022a, b), known as the Genesis Potential Parameter (*GPP*), is widely used across the globe for tropical cyclone studies (Kotal and Bhattacharya 2013; Paul et al. 2022). However, the requirement is to devise its extratropical counterpart, which encapsulates all the factors that impact the genesis location, frequency, and intensity of mid-latitude extratropical cyclones such as WDs.

The present study proposes a new parameter to identify the most active regions of mid-latitude cyclogenesis. It factors in some of the most critical parameters and

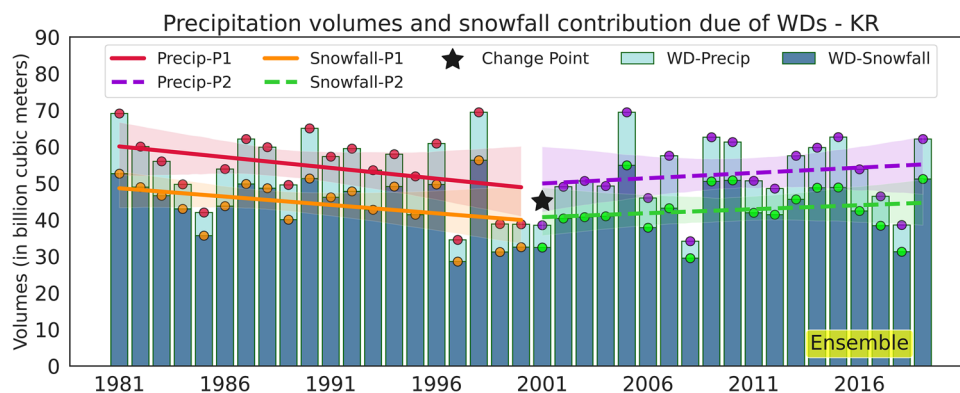
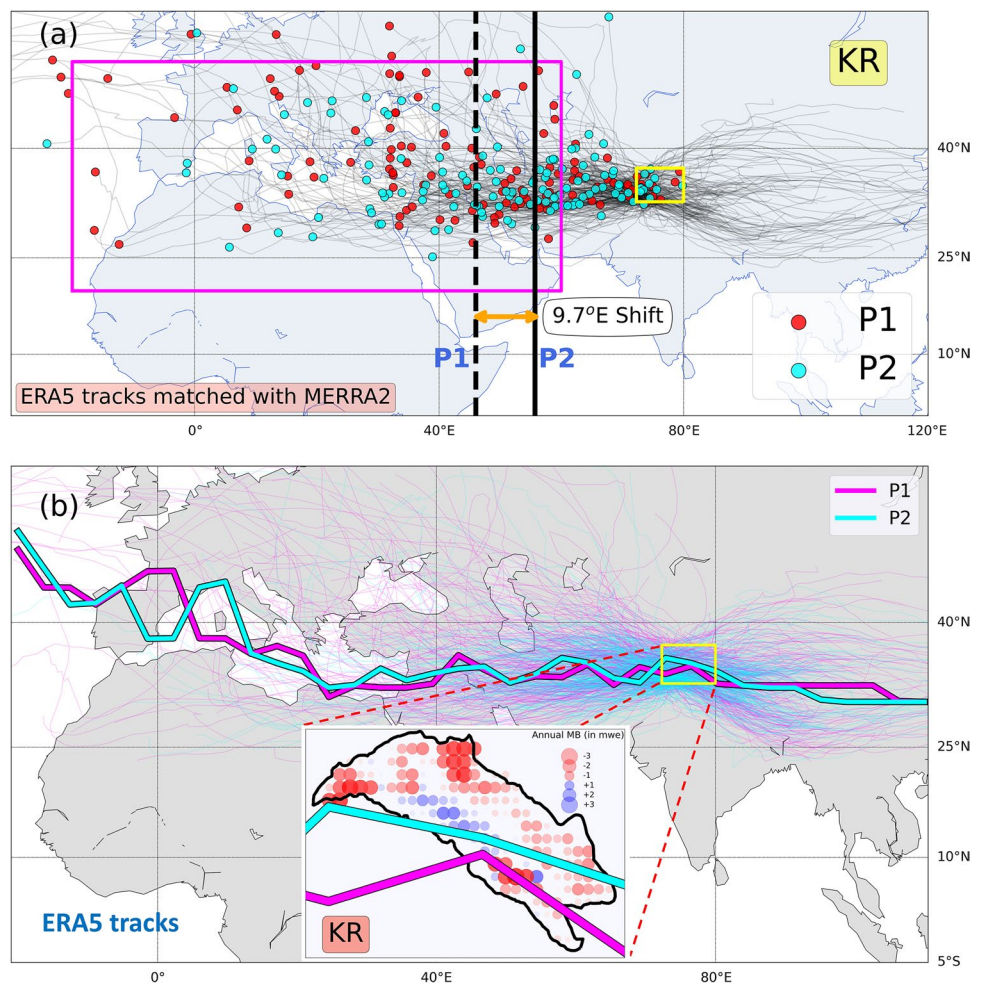


Fig. 2 Shows the contribution of snowfall in total precipitation received through WDs in Karakoram (in billion cubic meters). Black star represents the change point detected using Pettitt's test at 95% confidence interval. Solid lines depict the trends for total precipitation

and snowfall volumes during P1 (1980–2000) whereas dashed lines represent the same for P2 (2001–2019). The data shown is the ensemble mean of statistics generated for ERA5 and MERRA2 tracks

Fig. 3 **a** Shows the WD-tracks of ERA5 that matched with MERRA2 passing through the KR box (yellow). Red dots denote the genesis of P1 (1980–2000) WDs, whereas cyan dots denote the genesis of P2 (2001–2019) WDs. The black dashed line denotes the mean genesis longitude of P1 WDs, whereas the solid black line denotes the same for P2 WDs. **b** It shows the mean path of WDs during P1 (cyan) and P2 (magenta). The inset figure depicts the REMO_{glacier} simulated annual mass-balance of KR glaciers from 1989–2016 and provides the readers with visual evidence of the “Karakoram Anomaly” for their understanding (adapted from Kumar et al. 2019)



already-defined indices, such as *WDI* (Midhuna et al. 2020) and eady growth rate *egr* (Javed et al. 2022). While *WDI* considers the effects of geopotential anomaly, *egr* brings in the impact of baroclinicity. A modified version of *GPP* (symbolized by *mgpp*), slightly amended for studying upper tropospheric cyclonic systems, is also included. We will call this parameter as Mid-Latitude Genesis Potential (*MLGP*). The genesis tendency of a region is directly proportional to all the abovementioned factors and, therefore, *MLGP* is defined as:

$$MLGP = 3 * \bar{WDI} * \bar{egr} * \bar{mgpp}$$

Where the proportionality constant is taken to be equal to ‘3’ and the bar indicates normalized data calculated using the following procedure:

$$\bar{x} = \frac{mean(x) - \min(x)}{\max(x) - \min(x)}$$

Normalizing the data eliminates the associated units of all the parameters involved, leaving the resultant parameter unitless. It also ensures that all the input variables have the

same treatment in the calculation, removing redundancy and enhancing cohesion among the datasets. The proportionality constant is taken as ‘3’ to rescale the resultant parameter between 0 and 1. The details for calculating individual variables, including the equations involved and the datasets required for their calculations, are provided below.

3.5.1 Western Disturbance Index

Western Disturbance Index, or *WDI*, was introduced by (Midhuna et al. 2020) to corroborate the characteristics of WDs with their associated dynamics. It is formulated using the difference between 850 and 200 hPa geopotential height anomaly. The seasonal mean value of geopotential height anomaly at 850 and 200 hPa is calculated. The value at 850 hPa is subtracted from 200 hPa and then divided by the standard deviation to construct a standardized *WDI*. The study found that *WDI* correlated positively with the number of WDs in a season. However, the index requires more intense WD systems in a season to show a good correlation.

3.5.2 Eady Growth Rate

The maximum Eady growth rate (*egr*) measures baroclinic instability (Eady 1949). The *egr* (s^{-1}) is given by (Lindzen and Farrell 1980; Simmonds and Lim 2009; Vallis 2006):

$$egr = 0.3098 \frac{|fcor| \left| \frac{\partial U(z)}{\partial z} \right|}{N}$$

Where *fcor* is the Coriolis parameter, $U(z)$ is the vertical profile of the eastward wind component, z is the vertical coordinate, and N is the Brunt-Väisälä frequency given by:

$$N^2 = \frac{g}{\theta} \frac{\partial \theta}{\partial z}$$

Where g is the acceleration due to gravity, and θ is the potential temperature. The vertical derivatives are computed as a finite difference of values at 400 hPa and 300 hPa levels (Javed et al. 2022).

3.5.3 Modified Genesis Potential Parameter

A monthly modified version of the Genesis Potential Parameter (*GPP*), inspired by the works of (Kotal and Bhattacharya 2013; Paul et al. 2022), is used in the present study. The previous studies employed the method on a daily scale for North Indian Ocean tropical cyclones to study case-based scenarios. However, we have modified the parameter for the mid-latitude cyclogenesis to study on a seasonal scale. It is based on two thermodynamic (Relative humidity (RH) and temperature difference between lower and middle atmosphere) and two dynamic (relative vorticity and vertical wind shear) parameters. While the thermodynamic parameter RH represents the moisture availability in the atmosphere, the temperature difference between the lower and middle atmosphere governs the atmospheric instability required for developing a system. Higher values of relative vorticity (a dynamic parameter) facilitate enhanced convection, whereas lower values of vertical wind-shear support cyclone formation by reducing the loss of moisture and latent heat energy. The modified genesis potential parameter (denoted by *mgpp*) is calculated using the parameters mentioned above:

$$mgpp = \begin{cases} \frac{\xi * M * I}{S} & \text{if } \xi > 0, M > 0, \text{ and } I > 0 \\ 0 & \text{if } \xi \leq 0, M \leq 0, \text{ and } I \leq 0 \end{cases}$$

Where ‘ ξ ’ is the upper-level vertically averaged relative vorticity between 400 hPa and 300 hPa; ‘ M ’ is the mid-tropospheric RH defined by the formula $M = (RH-40)/30$, RH is the vertically averaged relative humidity between 700 hPa and 500 hPa levels. ‘ I ’ is the mid-tropospheric instability signified by the temperature difference ($^{\circ}C$) between 850 hPa

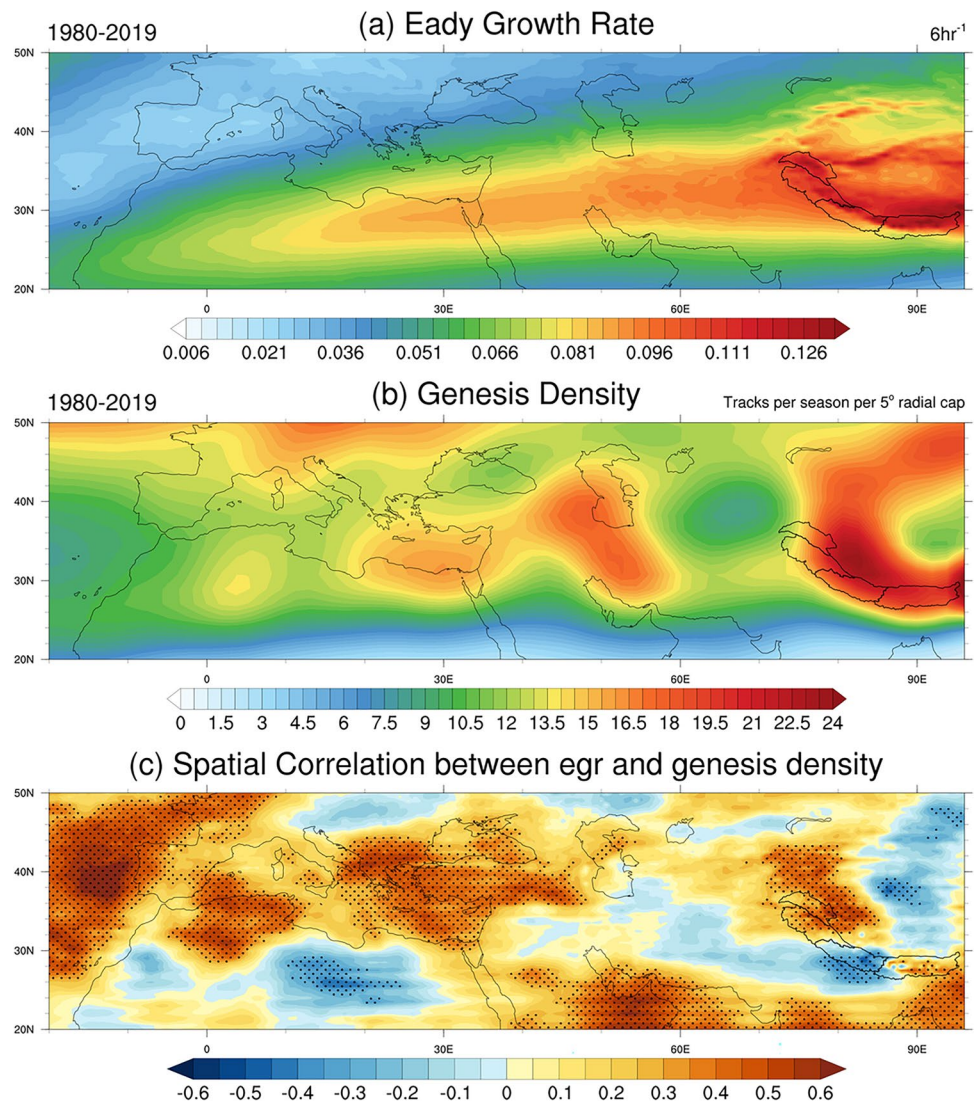
and 500 hPa, and ‘ S ’ is the vertical wind shear (computed as the vector difference between the 200 hPa and 850 hPa levels) of horizontal winds. The modified part is the temporal scale of the parameter calculated and the inclusion of upper tropospheric relative vorticity.

4 Results

4.1 Characteristics of the Core Genesis Zone and the Mean Path of WDs

Indian Meteorological Department (IMD) defines WDs as a “cyclonic circulation/trough in the mid to lower troposphere or as a low-pressure area at the surface, which occur in the mid-latitude westerlies and originate over the Mediterranean Sea, Caspian Sea, and the Black Sea and move eastward across north India” (<https://www.imdpune.gov.in/Reports/glossary.pdf>). The most striking feature observed in Fig. 3a is the noticeable eastward shift in the genesis locations of KR WDs. The clustered region can be called the core genesis zone (CGZ) of WDs and corresponds almost identically with a recent study that stated the region between $30^{\circ}E-61^{\circ}E$ as the most active genesis longitudes for WDs (Qiu et al. 2022). As will be discussed in detail later on, the mean genesis longitude shifted about $\sim 9.7^{\circ}E$ from $46^{\circ}E$ during P1 to $55.7^{\circ}E$ during P2, a significant ~ 950 km spatial shift in mean genesis locations. However, the majority still lies inside the original genesis box, largely complying with the IMD’s definition of a WD. Figure 3b shows the mean path of KR WDs for the two sub-periods. It reveals a slight poleward shift of the mean track over KR, essentially anchoring it almost adjacent to the glaciers with visible mass gain/stability (zoomed-in inset; Fig. 3b). The northward shift of the mean path can be attributed to the simultaneous poleward shift in the location of the STWJ. Some previous studies have established baroclinicity and the location of STWJ as the critical parameters controlling the frequency and genesis of the mid-latitude westerlies (Hunt et al. 2018b; Javed et al. 2022; Tierney et al. 2018). However, baroclinicity has a slight upper hand in controlling the WD occurrence frequencies during boreal winter (Dimri et al. 2015; Hunt et al. 2018a; Krishnan et al. 2019; Madhura et al. 2015). Figure 4 reiterates the findings of (Hunt et al. 2018a) and shows how upper-level baroclinicity facilitates and controls the genesis of mid-latitude westerlies of the Northern Hemisphere. Baroclinic instability (represented by eady growth rate, Fig. 4a) and genesis density (Fig. 4b) are found to be highly correlated with each other (Fig. 4c) in the last four decades. However, the regions of anti-correlation coincide with the supposed path of the STWJ, where the vertical wind shear is relatively intensified, thus negatively impacting the genesis of cyclones. Therefore, it can be said that STWJ has more

Fig. 4 **a** Ensemble mean of eady growth rate (averaged over 6 h⁻¹ temporal resolution for the months November–March each season) from 1980–2019. **b** Ensemble mean of genesis density of KR WDs **c** Spatial distribution of correlation between (a) and (b)

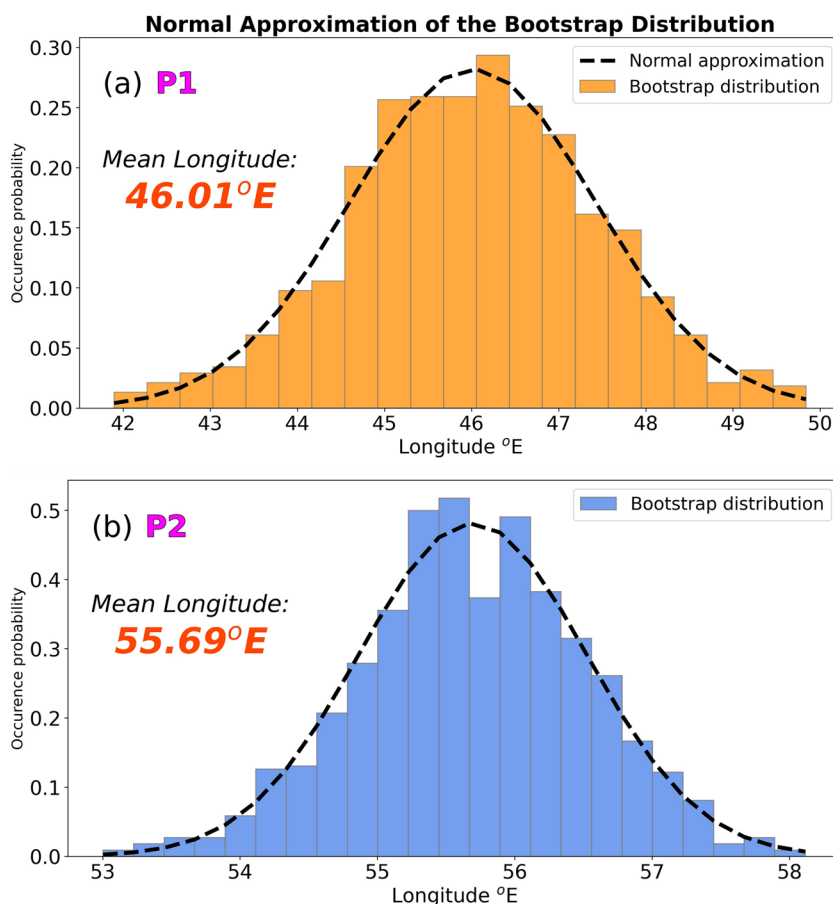


of a vehicular role in modulating the WD frequencies and lesser of a role in their genesis, helping them propagate eastward once they get embedded into the jet and dictating their path (Dimri et al. 2015; Hunt et al. 2018b; Krishnan et al. 2018). The details for the calculation of the eady growth rate are provided in the methodology Section 3.5.2.

The mean genesis longitudes for P1 and P2 were calculated by applying bootstrapping method to all the genesis locations in the respective sub-periods. The set of genesis longitudes were subjected to 1000 resampling iterations, eventually providing us with a normally distributed mean longitudes (Fig. 5). Bootstrapping is a non-parametric statistical test and does not rely on assumptions about the underlying distribution of the data. This makes it a valuable tool in situations where the distribution is unknown or complex. It involves randomly selecting samples with replacement from the observed data. Each bootstrap sample is the same size as the original dataset, but because it's

drawn with replacement, some observations may be repeated while others may be omitted. In Figs. 3 and 5, we used the actual genesis locations as the bootstrapping input to visualise the shift, whereas the Fig. 6 depicts the same using TRACK-generated spatial genesis density statistic. Figure 6a and b depict the inter-annual variability of the longitude of highest genesis density for P1 and P2, respectively. It is calculated using the genesis density values within 20°W–70°E and 20°N–50°N coordinates, covering the entirety of the genesis box up until the western edge of the KR box. The values are first meridionally averaged for each longitude, and the highest statistically weighted values (found using the loess regression technique) are joined together to form a smooth ribbon across the years. This technique identifies the most probable longitude for the existence of a genesis cluster and allows the ribbon to oscillate along the longitudes giving preference to the genesis centers having more statistical weight than the rest. The figures portray a noticeable

Fig. 5 Shows the normal approximation of the bootstrap distribution of TRACK-generated genesis longitudes for **a** P1 and **b** P2



downward shift of the ribbon, analogous to the eastward shift in the genesis activity of Karakoram WDs. The distribution of the mean genesis longitude, along with its kernel density estimation (KDE), is shown in Fig. 6c. The two periods display distinct distribution peaks, demonstrating the significant eastward shift in the CGZ. The difference between the two distributions was found to be highly statistically significant using the Kolmogorov-Smirnov test (at 1% level, p-value: 0.00146).

The consequences of such a shift can vary from impacting the anomaly region with more intense storms to even spatially shifting/extending the anomaly, especially when the presence of the anomaly is now already reported in western Kunlun (36°N, 84°E) and eastern Pamir ranges (38°N, 75°E) (Azam et al. 2018; Brun et al. 2017; Käab et al. 2015; Wang et al. 2017). Javed et al. 2022 had shown that the intensity of WDs impacting KR has increased without any change in their frequencies. It remains to be seen whether the zonal displacement of the core genesis region could explain the rise in intensities since the shift essentially moves them closer to the impact region, resulting in a shorter journey time and path. A hypothesis can also be found in a recent study that suggested shorter tracks produced in future climate simulations can negatively impact the spin-up of the

systems restricting their peak intensity before striking the Himalayas (Hunt et al. 2019b). However, it can be argued that the dynamics governing future WDs can vary significantly. The increased intensity of WDs or the rise in winter precipitation (Bolch et al. 2012; Dimri 2021; Farinotti et al. 2020; Javed et al. 2022) coupled with the nearing proximity of the storms (Fig. 3b) seems to facilitate the anomaly in recent decades.

4.2 Attributed Manifestations of the Shift and its Role in Modulating the Strength of WDs

Various factors can be attributed to the recent resurgence of WDs and the rise in associated precipitation over KR. Figure 7 depicts the mean monthly vertical cross-section (meridional mean between 20°N to 50°N) and the orography (sliced at the mean latitude for KR, i.e., 36°N) for some atmospheric parameters which can influence the genesis of WDs. The contours represent the sub-period difference (P2 minus P1) for the ensemble mean of ERA5 and MERRA2. The longitudinal extent is taken from 45°E (inspired by the mean genesis longitude during P1) to 85°E (slightly beyond the KR box). The idea is to investigate the region of highest genesis activity up to the impact region in question.

Fig. 6 Interannual variability (magenta ribbon) of the longitude of highest genesis density for **a** P1 and **b** P2. **c** The distribution of the mean genesis longitude along with their KDEs for P1 (red histogram, dotted curve) and P2 (blue histogram, solid curve)

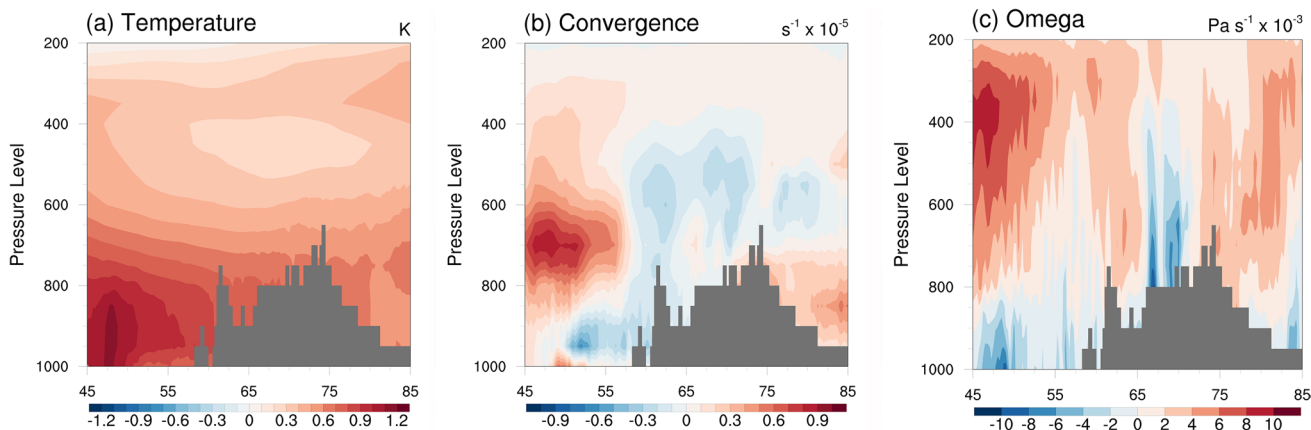
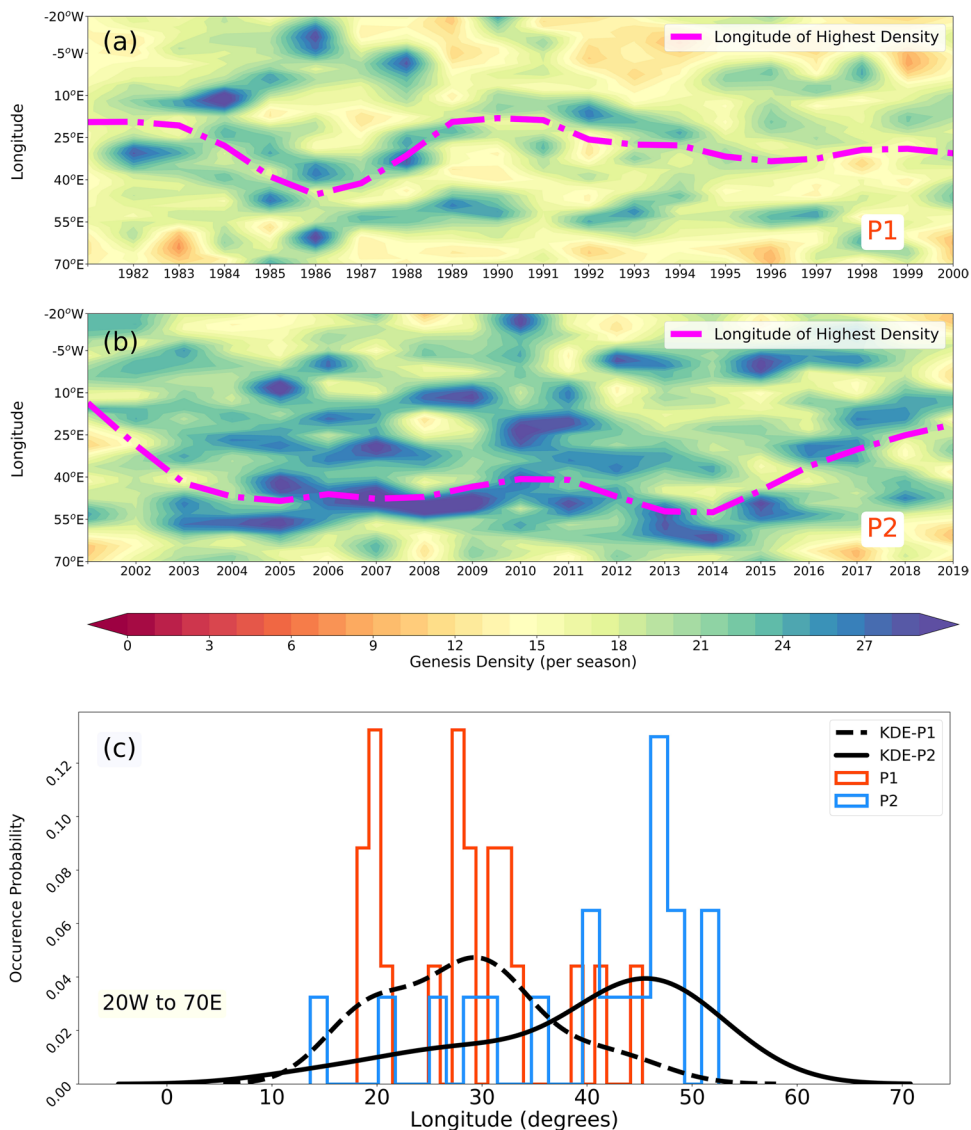


Fig. 7 **a** Shows the mean monthly vertical cross-section of temperature (zonal mean between 20°N to 50°N) and the orography (sliced at the mean latitude for KR, i.e., 36°N). **b** same as **a** but for convergence

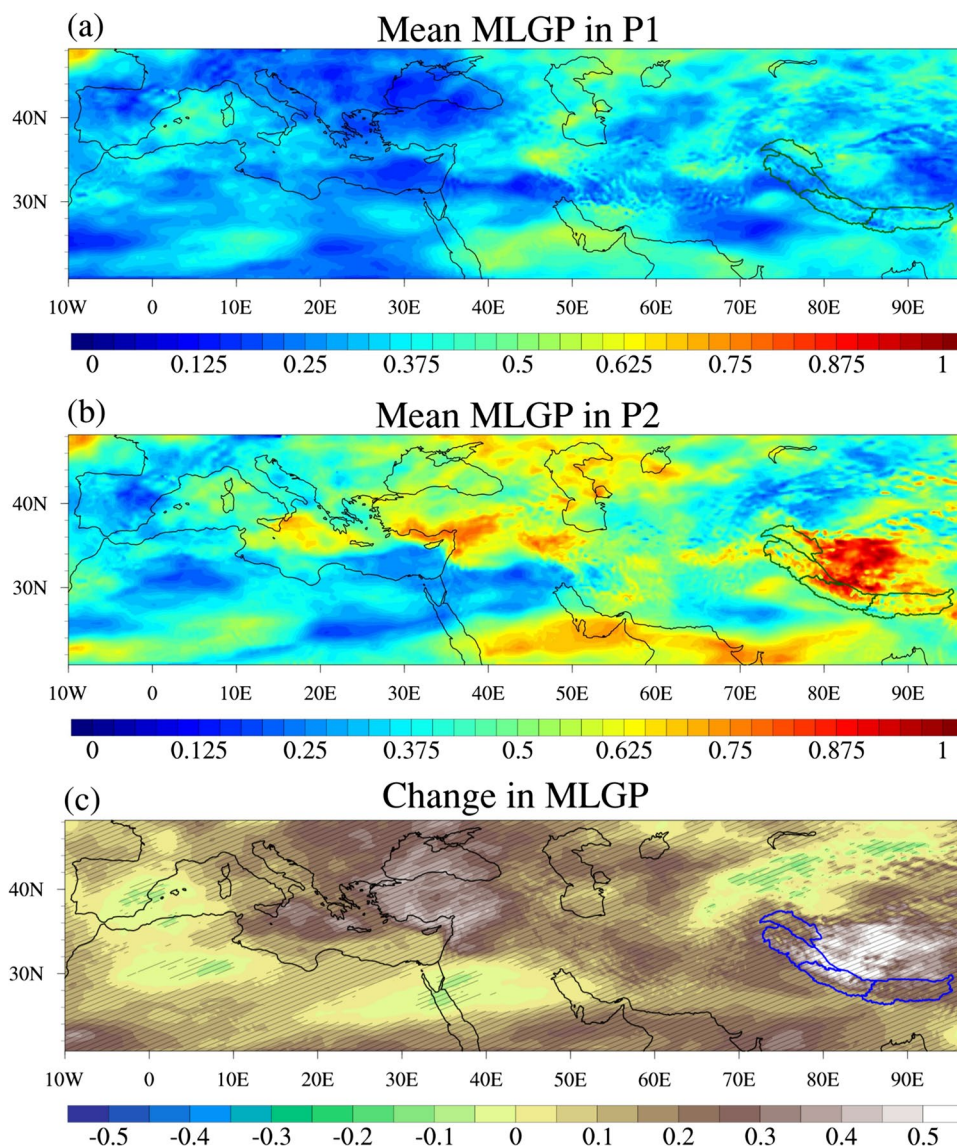
(s^{-1}). Negative values (blue contours) depict convergence. **c** same as **a** but for vertical velocity (omega) ($Pa s^{-1}$). Negative values (blue contours) depict upward motion/ascent

Distinct warming during P2 throughout the vertical section is observed in Fig. 7a. A warmer climate facilitates the heating of the surface air, which rises and creates a low-pressure region, inducing mass convergence (Fig. 7b; blue contours) and ascent (Fig. 7c; blue contours). The increased convergence found at lower pressure levels along the western longitudes coincides with the region of highest genesis activity (Figs. 3b and 4b).

The lobe of enhanced convergence continues along the western edge of High Mountain Asia, interacting constructively with the orography to produce the intense rainfall commonly associated with WDs (Baudouin et al. 2021; Hunt et al. 2018b). The intensified upward motion of air, especially near the periphery of KR, could partly explain the enhanced precipitation activity over the windward side of the KH (Bolch et al. 2012; Midhuna et al. 2020; Nie et al. 2021) since it is generally associated with the formation of clouds

and high precipitation activity. However, Fig. 8 provides a plausible reason for the significant shift in the genesis locations of WDs. It depicts a significant rise in the ensemble mean (ERA5 and MERRA2) of *MLGP* (Section 3.5) over the CGZ. The parameter has the potential to identify the regions with the highest genesis tendency. It incorporates factors influencing WDs' genesis, frequency, and intensity, such as geopotential height anomaly, zonal wind, air temperature, and available moisture at various pressure levels. Figure 8a and b shows the spatial distribution of the mean *MLGP* observed during P1 and P2. A significant rise in the genesis potential is observed over the eastward territorial land beyond 20°E, almost coinciding with the CGZ as well as the region of highest genesis tendency as shown in Fig. 4b. On the other hand, the rise is relatively subdued over the Mediterranean Sea (Fig. 8c). It should be noted that this does not mean that the genesis potential has decreased

Fig. 8 a Ensemble Mean *MLGP* in P1 b Ensemble Mean *MLGP* in P2 c Ensemble mean change (P2 minus P1) in *MLGP* for KR WDs. Hatchings denote significance at 5% level

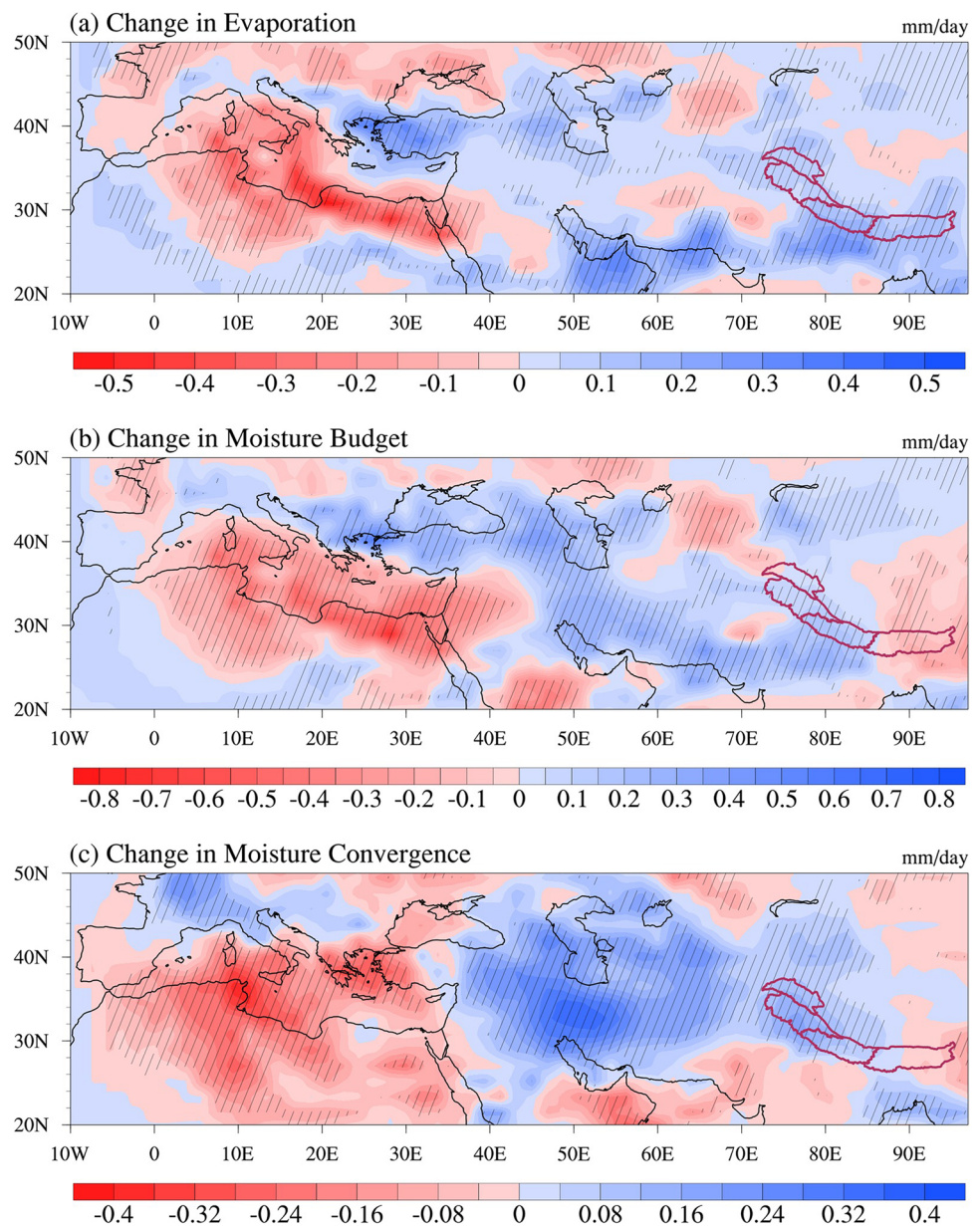


over the Mediterranean Sea. Instead, the territorial land has had more favourable conditions for cyclogenesis, ensuing in a significant shift in the genesis locations of WDs. It also highlights an interesting aspect of CGZ moving away from a primary moisture source which intuitively should result in weakened intensities of WDs. However, we explored some moisture parameters associated with WDs in a composite framework to unravel the sources of moisture.

The associated precipitation volume and intensity are already reported to have increased in P2 for tracks passing through KR (Javed et al. 2022). We investigate parameters such as evaporation, moisture budget (precipitation minus evaporation), and vertically integrated moisture convergence (Fig. 9). The presented results are ensemble mean composite

statistics. Figure 8a reveals the significant role of local moisture availability (evaporation) in intensifying the impact of WDs. Enhanced evaporation is observed throughout the path of WDs, right from the CGZ to the eventual impact region. A highly significant decline in evaporation is found over the Mediterranean Sea, whereas a statistically significant rise is observed over KR. It would be interesting to look into the sources of this enhanced evaporation availability across High Mountain Asia, especially when a sharp increase in the number of glacial lakes and their role in the amplification of evaporation has been reported for the region (Maurer et al. 2019; Song et al. 2020). However, a study has shown that local evaporation has little role to play in enhancing WD-precipitation, and significant contributors to moisture

Fig. 9 Change in the ensemble mean (P2 minus P1) for KR WDs **a** Evaporation **b** Moisture Budget **c** Vertically integrated moisture convergence. All in mm/day. Hatchings denote significance at 5% level



through evaporation processes are the Persian Gulf, the Red Sea, and the Arabian Sea (Baudouin et al. 2021). The WD-associated moisture budget, calculated using methods used in previous studies (Bengtsson et al. 2011; Vanni re et al. 2020), reveals very similar spatial patterns. A statistically significant decrease in the moisture budget over the Mediterranean Sea is succeeded by a significant rise over the CGZ (Fig. 9b). The enhanced moisture availability helps in the genesis of cyclones and provides positive feedback for their propagation (Catto 2016; Pfahl and Sprenger 2016; Wu et al. 2015). The zonal shift of genesis activity observed during P2 could result from this enhanced moisture budget all along the path of WDs up until the central part of the KH.

However, Fig. 9c provides a clearer picture of why the genesis activity tends to cluster closely over the terrestrial region east of the Mediterranean Sea in recent decades. The region has witnessed an enhanced moisture influx or convergence from nearby water bodies, including the Black Sea and the Red Sea. Moreover, the composite analysis suggests that the moisture divergence (red contours) has significantly increased over the Mediterranean Sea, similar to what was suggested by Fig. 9a and b. Therefore the CGZ, i.e., the region sandwiched between the Caspian Sea and the Persian Gulf, has experienced a highly significant rise in convergence, the region where the genesis cluster is denser during P2. It raises another question about the source of such moisture in the region despite moving away from a relatively more significant source (the Mediterranean Sea). However, it should be noted that the spatial patterns of decreasing convergence (and other moisture parameters) over the Mediterranean Sea do not correspond to a declining role in providing moisture. The Mediterranean Sea remains the primary source of moisture for WDs simply because of its areal extent and proximity. Readers should also remember that the results shown are composite analyses of WDs impacting KR, and the spatial patterns may vary significantly on the days when either no WD activity happens or on the days of WDs which do not impact KR.

Although most intense WDs originate over the Mediterranean Sea, the Arabian Sea has also been suggested as the reinforcing source of moisture during boreal winter (Midhuna et al. 2020), with relatively lesser input being provided by the Red Sea (Dimri 2007; Filippi et al. 2014), the Caspian Sea (Dimri and Niyogi 2013; Syed et al. 2010), and the Persian Gulf (Baudouin et al. 2021). The presence of moisture pathways drawing moisture from all the above-mentioned sources has also been reported in a recent study (Baudouin et al. 2021). The study also discussed the interactions of these pathways with WDs, highlighting the feedback mechanisms which can both intensify or inhibit the strength of WDs depending upon other synoptic circumstances. Another recent study suggested that the Mediterranean/Caspian Seas and the Mediterranean Land region (which

closely resembles the extent of our genesis box but without the water bodies) have dominant control over cold-season precipitation variability over high-mountain Asia and is responsible for nearly 50% of the total seasonal precipitation (Mehmood et al. 2022). The rest is divided to a lesser extent among the Indian Ocean, North Atlantic Ocean, and local recycling. It can be inferred from the composite analysis that the CGZ lies at optimum proximity to all the surrounding water bodies and draws significant moisture from them to have a sustained influx of moisture which could be one of the possible triggers for the eastward displacement of WDs genesis during P2.

Now the question arises whether or not the zonal displacement of the genesis cluster impacts WDs' intensity. This is important in the context of the "Karakoram Anomaly," as it is well established that WDs are the significant source of snowfall during the accumulation period of glaciers (Javed et al. 2022). Figure 10a depicts the vertical cross-section of the winter season zonal wind pattern (ensemble mean) change across the genesis box until the eastern edge of Karakoram. It clearly shows an increase in the eastbound wind speed over most of the Mediterranean Sea, which can facilitate the transport of moisture over the terrestrial land. The vertical cross-section depicts a change in sign (and direction) observed around 30°E longitude on the upper levels and slightly tilting westward as we approach the surface. The structure aligns almost perpendicular to the CGZ, suggesting it to be a confluence region for moisture-laden winds (Fig. 9c). The enhanced moisture availability thus becomes a crucial factor in the supposed eastward shift in the genesis locations.

Even though moisture has increased during P2, the shifting of genesis locations sounds counter-intuitive to the hypotheses of increasing intensities of KR WDs, mainly because of their migration away from the primary moisture source and the shortening of the track paths, which inhibits their spin-up time (Hunt et al. 2019b). However, Fig. 10b depicts the KR WDs' mean propagation speeds and reveals an interesting aspect. A statistically significant decline in the propagation speeds is observed along the WD-pathway, effectively providing more time for the systems to pick up the enhanced moisture available along the path and counter the effects of a shorter journey path. The decrease in propagation speeds may have allowed the systems sufficient time to spin up and intensify before colliding with the KH. Interestingly, the storms seem to spend less time over KR during P2, as shown in Fig. 10c, which depicts the number of hours WDs spend inside the KR box in a season. The "storm hours" have been steadily declining in the last four decades; however, a slight increase (not significant at the 5% level) is observed during P2. Despite increasing propagation speed and declining hours count within the KR box, the winter precipitation has increased in recent years (Javed et al. 2022;

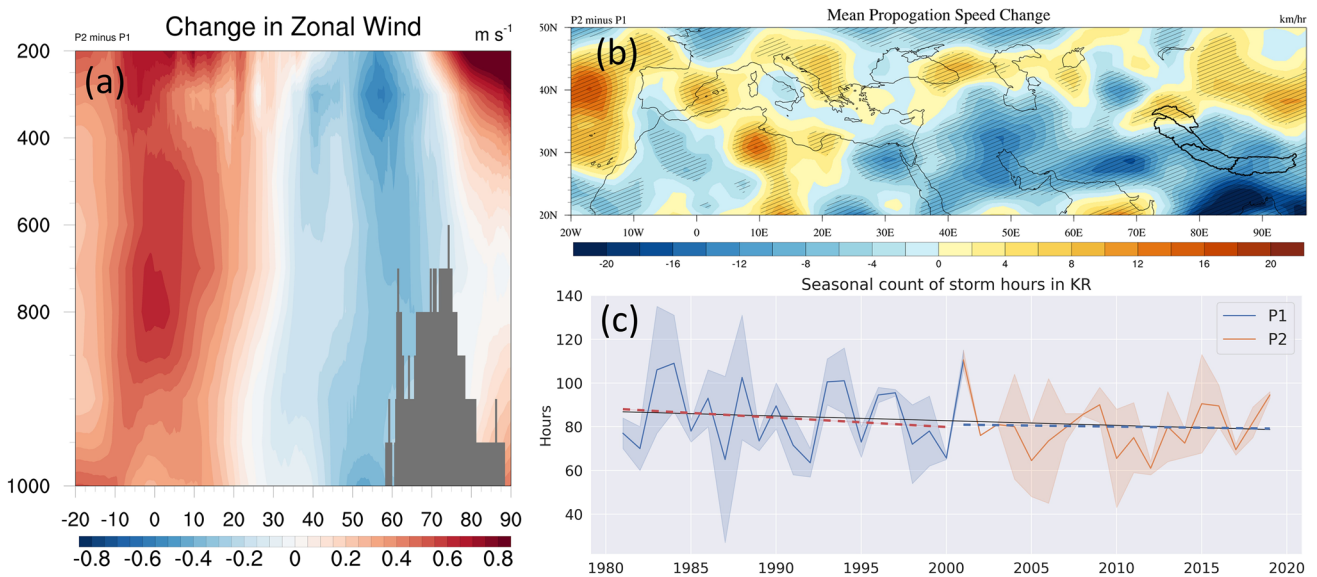


Fig. 10 **a** Vertical cross-section of the change in the zonal wind in P2 with respect to P1 (m s^{-1}) **b** Ensemble mean change (P2 minus P1) in the propagation speeds of KR WDs (km/hr). **c** Seasonal count of storm hours, i.e., hours spent by WDs inside the KR box in a season

Vishwakarma et al. 2022), also reported in various previous studies (Azam et al. 2021; Bolch et al. 2012; Dimri 2021), and reiterating the notion of increasing extreme precipitation events over the Karakoram in recent decades.

5 Conclusions

The present study strives to unearth the key features of the WDs passing through the Karakoram part of the KH (Fig. 1). We used the existing WD-catalog of Javed et al. 2022, prepared by applying a tracking algorithm to T63 spectrally filtered 3-hourly relative vorticity fields of ERA5 and MERRA2 between 300 and 400 hPa levels. The study period (1980–2019) was divided into sub-periods: P1 (1980–2000) and P2 (2001–2019), based on change point detection test (Fig. 2). We first filtered out the best-matched WD tracks passing through KR and observed a $\sim 9.7^\circ\text{E}$ shift in the core genesis zone (CGZ) during P2 (Fig. 3a). The mean path of WDs over KR is also found to have anchored itself closer to the anomalous glacial surge pockets (Fig. 3b). Genesis density of WDs were found to be highly correlated with the regions of high baroclinic instability (Fig. 4) in the last four decades. The mean genesis longitude for P1 and P2 were identified using bootstrapping technique, employed on the actual genesis locations generated by the tracking algorithm (Fig. 5). The inter-annual variability curve of the highest genesis density longitude portrays a noticeable downward shift, analogous to the eastward shift in the genesis activity of Karakoram WDs (Fig. 6a and b). The mean genesis longitude and their KDEs depict distinct distribution peaks,

statistically proving the significant eastward shift in the CGZ (Fig. 6c). The shift is possibly a by-product of a warmer climate, enhanced convergence, and more moisture availability around the core genesis cluster region (Fig. 7).

A new parameter called Mid-latitude Genesis Potential (*MLGP*) is proposed to identify regions of potential extratropical cyclogenesis. The mean change in *MLGP* during P2 suggests significant enhancement for cyclogenesis over the CGZ (Fig. 8c). Moisture parameters such as evaporation, moisture budget (precipitation minus evaporation), and vertically integrated moisture convergence have significantly risen over the CGZ in the recent period, not only fueling the genesis of WDs away from the Mediterranean Sea (Fig. 9) but intensifying the associated precipitation over the Karakoram. The decrease in propagation speeds of the systems (Fig. 10) counters the impact of shorter track paths due to the eastward shift in their genesis locations (which inhibits their spin-up and intensification process). Javed et al. 2022 showed that the WD-associated snowfall over KR has increased during P2, suggesting more extreme WD events over KR in the recent period, playing a crucial role in maintaining the health of “Karakoram Anomaly.” However, it remains to be seen whether the anomaly will cease to exist in the future if the core genesis zone of WDs continues to shift further east. A continuous migration may eventually lead to a tipping point where WDs may no longer be able to draw enough moisture from the sources, but these are still speculations and require thorough investigation.

Acknowledgements We acknowledge the unwavering help and support of Dr. Kevin Hodges, University of Reading, UK, for providing his

‘TRACK’ algorithm and constructive discussions to achieve the study’s objectives. AJ acknowledges the fellowship from the Indian Institute of Science Education and Research (IISER) Bhopal. PK acknowledges funding from Science and Engineering Research Board (SERB), Govt. of India, grant number CRG/2021/001227-G.

Declarations

Conflict of Interest The authors declare that they have no conflict of interest.

References

- Azam, M.F., Wagnon, P., Berthier, E., Vincent, C., Fujita, K., Kargel, J.S.: Review of the status and mass changes of Himalayan-Karakoram glaciers. *J. Glaciol.* **64**, 61–74 (2018). <https://doi.org/10.1017/jog.2017.86>
- Azam, M.F., Kargel, J.S., Shea, J.M., Nepal, S., Haritashya, U.K., Srivastava, S., Maussion, F., Qazi, N., Chevallier, P., Dimri, A.P., Kulkarni, A.V., Cogley, J.G., Bahuguna, I.: Glaciology of the Himalaya-Karakoram. *Science* (80-). **373**. (2021). <https://doi.org/10.1126/SCIENCE.ABF3668/ASSET/A27CFF34-2885-4961-B7DA-950FC19D8B7E/ASSETS/IMAGES/LARGE/SCIENCE.ABF3668-F4.JPG>
- Bashir, F., Zeng, X., Gupta, H., Hazenberg, P.: A hydrometeorological perspective on the Karakoram Anomaly using unique valley-based synoptic weather observations. *Geophys. Res. Lett.* **44**, 10,470–10,478 (2017). <https://doi.org/10.1002/2017GL075284>
- Baudouin, J.-P., Herzog, M., Petrie, C.A.: Synoptic processes of winter precipitation in the Upper Indus Basin. *Weather Clim. Dynam.* **2**, 1187–1207 (2021). <https://doi.org/10.5194/wcd-2-1187-2021>
- Bengtsson, L., Hodges, K.I., Koumoutsaris, S., Zahn, M., Keenlyside, N.: The changing atmospheric water cycle in Polar regions in a warmer climate. *Tellus Ser. Dyn. Meteorol. Oceanogr.* **63**, 907–920 (2011). <https://doi.org/10.1111/j.1600-0870.2011.00534.x>
- Berthier, E., Brun, F.: Karakoram geodetic glacier mass balances between 2008 and 2016: persistence of the anomaly and influence of a large rock avalanche on Siachen Glacier. *J. Glaciol.* **65**, 494–507 (2019). <https://doi.org/10.1017/JOG.2019.32>
- Bolch, T., Kulkarni, Kaab, Huggel, C., Paul, F., Cogley, J.G., Frey, H., Kargel, J.S., Fujita, K., Scheel, M., Bajracharya, S., Stoffel, M.: The state and fate of Himalayan glaciers. *Science* (80-). **336**, 310–314. (2012). <https://doi.org/10.1126/science.1215828>
- Brun, F., Berthier, E., Wagnon, P., Käab, A., Treichler, D.: A spatially resolved estimate of High Mountain Asia glacier mass balances, 2000–2016. *Nat. Geosci.* (2017). <https://doi.org/10.1038/ngeo2999>
- Cannon, F., Carvalho, L.M.V., Jones, C., Bookhagen, B.: Multi-annual variations in winter westerly disturbance activity affecting the Himalaya. *Clim. Dyn.* **44**, 441–455 (2015). <https://doi.org/10.1007/s00382-014-2248-8>
- Cannon, F., Carvalho, L.M.V., Jones, C., Norris, J.: Winter westerly disturbance dynamics and precipitation in the western Himalaya and Karakoram: A wave-tracking approach. *Theor. Appl. Climatol.* **125**, 27–44 (2016). <https://doi.org/10.1007/s00704-015-1489-8>
- Catto, J.L.: Extratropical cyclone classification and its use in climate studies. *Rev. Geophys.* **54**, 486–520 (2016). <https://doi.org/10.1002/2016RG000519>
- Copernicus Climate Change Service (C3S): ERA5: Fifth generation of ECMWF atmospheric reanalyses of the global climate. Copernicus Clim. Chang. Serv. Clim. Data Store (CDS). (2017). <https://cds.climate.copernicus.eu/cdsapp#!/home>. Accessed 05-04-2018
- Curio, J., Schiemann, R., Hodges, K.I., Turner, A.G.: Climatology of Tibetan Plateau vortices in reanalysis data and a high-resolution global climate model. *J. Clim.* **32**, 1933–1950 (2019). <https://doi.org/10.1175/JCLI-D-18-0021.1>
- de Kok, R.J., Tuinenburg, O.A., Bonekamp, P.N.J., Immerzeel, W.W.: Irrigation as a potential driver for Anomalous Glacier Behavior in High Mountain Asia. *Geophys Res Lett* **45**, 2047–2054 (2018). <https://doi.org/10.1002/2017GL076158>
- Dee, D.P., Uppala, S.M., Simmons, A.J., Berrisford, P., Poli, P., Kobayashi, S., Andrae, U., Balmaseda, M.A., Balsamo, G., Bauer, P., Bechtold, P., Beljaars, A.C.M., van de Berg, L., Bidlot, J., Bormann, N., Delsol, C., Dragani, R., Fuentes, M., Geer, A.J., Haimberger, L., Healy, S.B., Hersbach, H., Hólm, E.V., Isaksen, I., Kållberg, P., Köhler, M., Matricardi, M., McNally, A.P., Monge-Sanz, B.M., Morcrette, J.-J., Park, B.-K., Peubey, C., de Rosnay, P., Tavolato, C., Thépaut, J.-N., Vitart, F.: The ERA-Interim reanalysis: configuration and performance of the data assimilation system. *Q. J. R. Meteorol. Soc.* **137**, 553–597 (2011). <https://doi.org/10.1002/qj.828>
- Dehecq, A., Gourmelen, N., Gardner, A.S., Brun, F., Goldberg, D., Nienow, P.W., Berthier, E., Vincent, C., Wagnon, P., Trouvé, E.: Twenty-first century glacier slowdown driven by mass loss in High Mountain Asia. *Nat Geosci* **12**, 22–27 (2019). <https://doi.org/10.1038/s41561-018-0271-9>
- Dimri, A.P.: The transport of momentum, sensible heat, potential energy and moisture over the western Himalayas during the winter season. *Theor Appl Climatol* **90**, 49–63 (2007). <https://doi.org/10.1007/s00704-006-0274-0>
- Dimri, A.P.: Decoding the Karakoram Anomaly. *Sci Total Environ* **788**, 147864 (2021). <https://doi.org/10.1016/J.SCITOTENV.2021.147864>
- Dimri, A.P., Chevuturi, A.: Model sensitivity analysis study for western disturbances over the Himalayas. *Meteorol Atmos Phys* **123**, 155–180 (2014). <https://doi.org/10.1007/s00703-013-0302-4>
- Dimri, A.P., Niyogi, D.: Regional climate model application at sub-grid scale on Indian winter monsoon over the western Himalayas. *Int J Climatol* **33**, 2185–2205 (2013). <https://doi.org/10.1002/joc.3584>
- Dimri, A.P., Niyogi, D., Barros, A.P., Ridley, J., Mohanty, U.C., Yasunari, T., Sikka, D.R.: Western disturbances: A review. *Rev Geophys* **53**, 225–246 (2015). <https://doi.org/10.1002/2014RG000460>
- Eady, E.T.: Long waves and Cyclone waves. *Tellus* **1**, 33–52 (1949). <https://doi.org/10.1111/j.2153-3490.1949.tb01265.x>
- Farinotti, D., Immerzeel, W.W., de Kok, R.J., Quincey, D.J., Dehecq, A.: Manifestations and mechanisms of the Karakoram glacier anomaly. *Nat Geosci* **13**, 8–16 (2020). <https://doi.org/10.1038/s41561-019-0513-5>
- Filippi, L., Palazzi, E., Von Hardenberg, J., Provenzale, A.: Multidecadal variations in the relationship between the NAO and Winter Precipitation in the Hindu Kush–Karakoram. *J Clim* **27**, 7890–7902 (2014). <https://doi.org/10.1175/JCLI-D-14-00286.1>
- Forsythe, N., Fowler, H.J., Li, X.F., Blenkinsop, S., Pritchard, D.: Karakoram temperature and glacial melt driven by regional atmospheric circulation variability. *Nat Clim Chang* **7**, 664–670 (2017). <https://doi.org/10.1038/nclimate3361>
- Fowler, H.J., Archer, D.R.: Conflicting signals of climatic change in the Upper Indus Basin. *J Clim* **19**, 4276–4293 (2006). <https://doi.org/10.1175/JCLI3860.1>
- Frey, H., Machguth, H., Huss, M., Huggel, C., Bajracharya, S., Bolch, T., Kulkarni, A., Linsbauer, A., Salzmann, N., Stoffel, M.: Estimating the volume of glaciers in the Himalayan-Karakoram region using different methods. *Cryosphere* **8**, 2313–2333 (2014). <https://doi.org/10.5194/tc-8-2313-2014>
- Gardelle, J., Berthier, E., Arnaud, Y.: Slight mass gain of Karakoram glaciers in the early twenty-first century. *Nat Geosci* **5**, 322–325 (2012). <https://doi.org/10.1038/ngeo1450>

- Gelaro, R., McCarty, W., Suárez, M.J., Todling, R., Molod, A., Takacs, L., Randles, C.A., Darmenov, A., Bosilovich, M.G., Reichle, R., Wargan, K., Coy, L., Cullather, R., Draper, C., Akella, S., Buchard, V., Conaty, A., da Silva, A.M., Gu, W., Kim, G.K., Koster, R., Lucchesi, R., Merkova, D., Nielsen, J.E., Partyka, G., Pawson, S., Putman, W., Rienecker, M., Schubert, S.D., Sienkiewicz, M., Zhao, B.: The modern-era retrospective analysis for research and applications, version 2 (MERRA-2). *J Clim* **30**, 5419–5454 (2017). <https://doi.org/10.1175/JCLI-D-16-0758.1>
- Hersbach, H., Bell, W., Berrisford, P., Horányi, A.A., Nicolas, J.M.-S., Radu, J., Schepers, R., Simmons, D., Soci, A., Dee, C., Bell, D., Berrisford, B., Horányi, P., Sabater, A.A., Nicolas, J.M., Radu, J., Schepers, R., Simmons, D., Soci, A., Dee, C.: D.: Global reanalysis: Goodbye ERA-Interim, hello ERA5. *ECMWF Newsl.* 17–24. (2019). <https://doi.org/10.21957/vf291hehd7>
- Hodges, K., Cobb, A., Vidale, P.L.: How well are Tropical cyclones represented in Reanalysis datasets? *J Clim* **30**, 5243–5264 (2017). <https://doi.org/10.1175/JCLI-D-16-0557.1>
- Hunt, K., Zaz, S.N.: Linking the North Atlantic Oscillation to winter precipitation over the Western Himalaya through disturbances of the subtropical jet. *Clim. Dyn.* **1**, 1–15 (2022). <https://doi.org/10.1007/S00382-022-06450-7/TABLES/1>
- Hunt, K., Curio, J., Turner, A.G., Schiemann, R.: Subtropical Westerly Jet Influence on occurrence of western disturbances and tibetan Plateau vortices. *Geophys. Res. Lett.* **45**, 8629–8636 (2018a). <https://doi.org/10.1029/2018GL077734>
- Hunt, K., Turner, A.G., Shaffrey, L.C.: The evolution, seasonality and impacts of western disturbances. *Q. J. R. Meteorol. Soc.* **144**, 278–290 (2018b). <https://doi.org/10.1002/QJ.3200>
- Hunt, K., Turner, A.G., Shaffrey, L.C.: Representation of western disturbances in CMIP5 models. *J. Clim.* **32**, 1997–2011 (2019a). <https://doi.org/10.1175/JCLI-D-18-0420.1>
- Hunt, K., Turner, A.G., Shaffrey, L.C.: Falling trend of western disturbances in future climate simulations. *J. Clim.* **32**, 5037–5051 (2019b). <https://doi.org/10.1175/JCLI-D-18-0601.1>
- Jacob, D., Podzun, R.: Sensitivity studies with the regional climate model REMO. *Meteorol. Atmos. Phys.* 1997 **631** **63**, 119–129 (1997). <https://doi.org/10.1007/BF01025368>
- Javed, A., Kumar, P., Hodges, K.I., Sein, D.V., Dubey, A.K., Tiwari, G.: Does the recent Revival of Western disturbances govern the Karakoram Anomaly? *J Clim* **35**, 4383–4402 (2022). <https://doi.org/10.1175/JCLI-D-21-0129.1>
- Javed, A., Anshuman, K., Kumar, P., Sachan, D.: The decline in western disturbance activity over Northern India in recent decades. *Clim Change* **176**, 1–22 (2023). <https://doi.org/10.1007/s10584-023-03571-8>
- Kääb, A., Treichler, D., Nuth, C., Berthier, E.: Brief communication: contending estimates of 2003–2008 glacier mass balance over the Pamir-Karakoram-Himalaya. *Cryosphere* **9**, 557–564 (2015). <https://doi.org/10.5194/tc-9-557-2015>
- Kapnick, S.B., Delworth, T.L., Ashfaq, M., Malyshev, S., Milly, P.C.D.: Snowfall less sensitive to warming in Karakoram than in Himalayas due to a unique seasonal cycle. *Nat Geosci* **7**, 834–840 (2014). <https://doi.org/10.1038/ngeo2269>
- Kotal, S.D., Bhattacharya, S.K.: Tropical cyclone genesis potential parameter (GPP) and its application over the north Indian sea. *Mausam* **64**, 149–170 (2013). <https://doi.org/10.54302/mausam.v64i1.663>
- Kotlarski, S.: A subgrid glacier parameterisation for use in regional climate modelling. *Rep. Earth Syst. Sci.* (2007). <https://doi.org/10.17617/2.994357>
- Kotlarski, S., Jacob, D., Podzun, R., Paul, F.: Representing glaciers in a regional climate model. *Clim Dyn* **34**, 27–46 (2010). <https://doi.org/10.1007/s00382-009-0685-6>
- Krishnan, R., Sabin, T.P., Madhura, R.K., Vellore, R.K., Mujumdar, M., Sanjay, J., Nayak, S., Rajeevan, M.: Non-monsoonal precipitation response over the Western Himalayas to climate change. *Clim. Dyn.* **527**(52), 4091–4109 (2018). <https://doi.org/10.1007/S00382-018-4357-2>
- Krishnan, R., Shrestha, A.B., Ren, G., Rajbhandari, R., Saeed, S., Sanjay, J., Syed, M.A., Vellore, R., Xu, Y., You, Q., Ren, Y.: Unravelling climate change in the Hindu Kush Himalaya: Rapid warming in the mountains and increasing extremes. In: Wester, P., Mishra, A., Mukherji, A., Shrestha, A., Bhakta (eds.) *The Hindu Kush Himalaya Assessment: Mountains, Climate Change, Sustainability and People*, pp. 57–97. Springer International Publishing, Cham (2019). https://doi.org/10.1007/978-3-319-92288-1_3
- Kumar, P., Kotlarski, S., Moseley, C., Sieck, K., Frey, H., Stoffel, M., Jacob, D.: Response of Karakoram-Himalayan glaciers to climate variability and climatic change: a regional climate model assessment. *Geophys Res Lett* **42**, 1818–1825 (2015). <https://doi.org/10.1002/2015GL063392>
- Kumar, P., Saharwardi, M.S., Banerjee, A., Azam, M.F., Dubey, A.K., Murtugudde, R.: Snowfall variability dictates Glacier Mass Balance variability in Himalaya-Karakoram. *Sci Rep* **9**, 18192 (2019). <https://doi.org/10.1038/s41598-019-54553-9>
- Lang, T.J., Barros, A.P.: Winter storms in the Central Himalayas. *J. Meteorol. Soc. Japan Ser. II* **82**, 829–844 (2004). <https://doi.org/10.2151/JMSJ.2004.829>
- Li, X.F., Fowler, H.J., Forsythe, N., Blenkinsop, S., Pritchard, D.: The Karakoram/Western Tibetan vortex: Seasonal and year-to-year variability. *Clim. Dyn.* **0**, 1–24 (2018). <https://doi.org/10.1007/s00382-018-4118-2>
- Lindzen, R.S., Farrell, B.: A simple approximate result for the Maximum Growth Rate of Baroclinic instabilities. *J Atmos Sci* **37**, 1648–1654 (1980). [https://doi.org/10.1175/1520-0469\(1980\)037%3c1648:ASARFT%3e2.0.CO;2](https://doi.org/10.1175/1520-0469(1980)037%3c1648:ASARFT%3e2.0.CO;2)
- Madhura, R.K., Krishnan, R., Revadekar, J.V., Mujumdar, M., Goswami, B.N.: Changes in western disturbances over the Western Himalayas in a warming environment. *Clim. Dyn.* **44**, 1157–1168 (2015). <https://doi.org/10.1007/S00382-014-2166-9/FIGURES/9>
- Maurer, J.M., Schaefer, J.M., Rupper, S., Corley, A.: Acceleration of ice loss across the Himalayas over the past 40 years. *Sci. Adv.* **5**, eaav7266 (2019). <https://doi.org/10.1126/sciadv.aav7266>
- Mehmood, S., Ashfaq, M., Kapnick, S., Gosh, S., Abid, M.A., Kucharski, F., Batibeniz, F., Saha, A., Evans, K., Hsu, H.-H.: Dominant controls of cold-season precipitation variability over the high mountains of Asia. *Npj Clim. Atmos. Sci.* **5**, 65 (2022). <https://doi.org/10.1038/s41612-022-00282-2>
- Midhuna, T.M., Kumar, P., Dimri, A.P.: A new western disturbance index for the Indian winter monsoon. *J Earth Syst Sci* **129**, 59 (2020). <https://doi.org/10.1007/s12040-019-1324-1>
- Mölg, T., Maussion, F., Scherer, D.: Mid-latitude westerlies as a driver of glacier variability in monsoonal high Asia. *Nat Clim Chang* **4**, 68–73 (2014). <https://doi.org/10.1038/nclimate2055>
- Mukhopadhyay, B., Khan, A.: Rising river flows and glacial mass balance in central Karakoram. *J Hydrol* **513**, 192–203 (2014). <https://doi.org/10.1016/j.jhydrol.2014.03.042>
- Negi, H.S., Kumar, A., Kanda, N., Thakur, N.K., Singh, K.K.: Status of glaciers and climate change of East Karakoram in early twenty-first century. *Sci Total Environ* **753**, 141914 (2021). <https://doi.org/10.1016/j.scitotenv.2020.141914>
- Nie, Y., Pritchard, H.D., Liu, Q., Hennig, T., Wang, W., Wang, X., Liu, S., Samyn, D., Hewitt, K., Chen, X.: Glacial change and hydrological. *Nat. Rev. Earth Environ.* (2021). <https://doi.org/10.1038/s43017-020-00124-w>
- Norris, J., Carvalho, L.M.V., Jones, C., Cannon, F.: WRF simulations of two extreme snowfall events associated with contrasting extratropical cyclones over the western and central Himalaya. *J Geophys Res* **120**, 3114–3138 (2015). <https://doi.org/10.1002/2014JD022592>



- Norris, J., Carvalho, L.M.V., Jones, C., Cannon, F., Bookhagen, B., Palazzi, E., Tahir, A.A.: The spatiotemporal variability of precipitation over the Himalaya: Evaluation of one-year WRF model simulation. *Clim Dyn* **49**, 2179–2204 (2017). <https://doi.org/10.1007/s00382-016-3414-y>
- Norris, J., Carvalho, L.M.V., Jones, C., Cannon, F.: Deciphering the contrasting climatic trends between the central Himalaya and Karakoram with 36 years of WRF simulations. *Clim Dyn* **0**, 1–22 (2018). <https://doi.org/10.1007/s00382-018-4133-3>
- Paul, D., Panda, J., Routray, A.: Ocean and atmospheric characteristics associated with the cyclogenesis and rapid intensification of NIO super cyclonic storms during 1981–2020. *Nat Hazards* (2022). <https://doi.org/10.1007/s11069-022-05389-6>
- Pfahl, S., Sprenger, M.: On the relationship between extratropical cyclone precipitation and intensity. *Geophys Res Lett* **43**, 1752–1758 (2016). <https://doi.org/10.1002/2016GL068018>
- Pfeffer, W.T., Arendt, A.A., Bliss, A., Bolch, T., Cogley, J.G., Gardner, A.S., Hagen, J.O., Hock, R., Kaser, G., Kienholz, C., Miles, E.S., Moholdt, G., Mölg, N., Paul, F., Radić, V., Rastner, P., Raup, B.H., Rich, J., Sharp, M.J., Andreassen, L.M., Bajracharya, S., Barrand, N.E., Beedle, M.J., Berthier, E., Bhambri, R., Brown, I., Burgess, D.O., Burgess, E.W., Cawkwell, F., Chinn, T., Copland, L., Cullen, N.J., Davies, B., De Angelis, H., Fountain, A.G., Frey, H., Giffen, B.A., Glasser, N.F., Gurney, S.D., Hagg, W., Hall, D.K., Haritashya, U.K., Hartmann, G., Herreid, S., Howat, I., Jiskoot, H., Khromova, T.E., Klein, A., Kohler, J., König, M., Kriegel, D., Kutuzov, S., Lavrentiev, I., Le Bris, R., Li, X., Manley, W.F., Mayer, C., Menounos, B., Mercer, A., Mool, P., Negrete, A., Nosenko, G., Nuth, C., Osmonov, A., Pettersson, R., Racoviteanu, A., Ranzi, R., Sarikaya, M.A., Schneider, C., Sigurdsson, O., Sirguey, P., Stokes, C.R., Wheate, R., Wolken, G.J., Wu, L.Z., Wyatt, F.R.: The Randolph glacier inventory: A globally complete inventory of glaciers. *J. Glaciol.* **60**, 537–552 (2014). <https://doi.org/10.3189/2014JoG13J176>
- Pinheiro, H.R., Hodges, K.I., Gan, M.A.: Sensitivity of identifying cut-off lows in the Southern Hemisphere using multiple criteria: Implications for numbers, seasonality and intensity. *Clim Dyn* **53**, 6699–6713 (2019). <https://doi.org/10.1007/s00382-019-04984-x>
- Priestley, M.D.K., Catto, J.L.: Future changes in the extratropical storm tracks and cyclone intensity, wind speed, and structure. *Weather Clim. Dyn.* **3**, 337–360 (2022). <https://doi.org/10.5194/wcd-3-337-2022>
- Qiu, T., Huang, W., Wright, J.S., Yang, Z., Wang, B.: Impacts of western disturbances on Wintertime Precipitation over the Southeastern Tibetan Plateau. *J. Geophys. Res. Atmos.* **127**, 1–17 (2022). <https://doi.org/10.1029/2021JD035789>
- Quincey, D.J., Braun, M., Glasser, N.F., Bishop, M.P., Hewitt, K., Luckman, A.: Karakoram glacier surge dynamics. *Geophys. Res. Lett.* **38**, 18504 (2011). <https://doi.org/10.1029/2011GL049004>
- Rienecker, M.M., Suarez, M.J., Gelaro, R., Todling, R., Bacmeister, J., Liu, E., Bosilovich, M.G., Schubert, S.D., Takacs, L., Kim, G.K., Bloom, S., Chen, J., Collins, D., Conaty, A., Da Silva, A., Gu, W., Joiner, J., Koster, R.D., Lucchesi, R., Molod, A., Owens, T., Pawson, S., Pegion, P., Redder, C.R., Reichle, R., Robertson, F.R., Ruddick, A.G., Sienkiewicz, M., Woollen, J.: MERRA: NASA's modern-era retrospective analysis for research and applications. *J. Clim* **24**, 3624–3648 (2011). <https://doi.org/10.1175/JCLI-D-11-00015.1>
- Romshoo, S.A., Fayaz, M., Meraj, G., Bahuguna, I.M.: Satellite-observed glacier recession in the Kashmir Himalaya, India, from 1980 to 2018. *Environ Monit Assess* **192**, 1–17 (2020). <https://doi.org/10.1007/S10661-020-08554-1/FIGURES/11>
- Romshoo, S.A., Abdullah, T., Rashid, I., Bahuguna, I.M.: Explaining the differential response of glaciers across different mountain ranges in the north-western Himalaya, India. *Cold Reg Sci Technol* **196**, 103515 (2022). <https://doi.org/10.1016/J.COLDREGIONS.2022.103515>
- Simmonds, I., Lim, E.P.: Biases in the calculation of Southern Hemisphere mean baroclinic eddy growth rate. *Geophys. Res. Lett.* **36** (2009). <https://doi.org/10.1029/2008GL036320>
- Song, C., Sheng, Y., Zhan, S., Wang, J., Ke, L., Liu, K.: Impact of amplified evaporation due to lake expansion on the water budget across the inner Tibetan Plateau. *Int J Climatol* **40**, 2091–2105 (2020). <https://doi.org/10.1002/joc.6320>
- Syed, F.S., Giorgi, F., Pal, J.S., Keay, K.: Regional climate model simulation of winter climate over central-southwest Asia, with emphasis on NAO and ENSO effects. *Int J Climatol* **30**, 220–235 (2010). <https://doi.org/10.1002/joc.1887>
- Tierney, G., Posselt, D.J., Booth, J.F.: An examination of extratropical cyclone response to changes in baroclinicity and temperature in an idealized environment. *Clim. Dyn.* (2018). <https://doi.org/10.1007/s00382-018-4115-5>
- Tiwari, G., Kumar, P., Javed, A., Mishra, A.K., Routray, A.: Assessing tropical cyclones characteristics over the Arabian Sea and Bay of Bengal in the recent decades. *Meteorol. Atmos. Phys.* **134**, 1–15 (2022a). <https://doi.org/10.1007/S00703-022-00883-9/FIGURES/12>
- Tiwari, G., Rameshan, A., Kumar, P., Javed, A., Mishra, A.K.: Understanding the post-monsoon tropical cyclone variability and trend over the Bay of Bengal during the satellite era. *Q J R Meteorol Soc* **148**, 1–14 (2022b). <https://doi.org/10.1002/qj.4189>
- Vallis, G.K.: Atmospheric and Oceanic Fluid Dynamics, Atmospheric and Oceanic Fluid Dynamics. (2006). <https://doi.org/10.1017/cbo9780511790447>
- Vannière, B., Roberts, M., Vidale, P.L., Hodges, K., Demory, M.E., Caron, L.P., Scoccimarro, E., Terray, L., Senan, R.: The moisture budget of tropical cyclones in HighResMIP models: large-scale environmental balance and sensitivity to horizontal resolution. *J. Clim* **33**, 8457–8474 (2020). <https://doi.org/10.1175/JCLI-D-19-0999.1>
- Vishwakarma, B.D., Ramsankaran, R.A.A.J., Azam, M.F., Bolch, T., Mandal, A., Srivastava, S., Kumar, P., Sahu, R., Navinkumar, P.J., Tanniru, S.R., Javed, A., Soheb, M., Dimri, A.P., Yadav, M., Devaraju, B., Chinnasamy, P., Reddy, M.J., Murugesan, G.P., Arora, M., Jain, S.K., Ojha, C.S.P., Harrison, S., Bamber, J.: Challenges in understanding the variability of the Cryosphere in the Himalaya and its impact on regional water resources. *Front. Water.* **4**, 102 (2022). <https://doi.org/10.3389/FRWA.2022.909246/BIBTEX>
- Wang, Q., Yi, S., Sun, W.: Precipitation-driven glacier changes in the Pamir and Hindu Kush mountains. *Geophys. Res. Lett.* **44**, 2817–2824 (2017). <https://doi.org/10.1002/2017GL072646>
- Wu, L., Su, H., Fovell, R.G., Dunkerton, T.J., Wang, Z., Kahn, B.H.: Impact of environmental moisture on tropical cyclone intensification. *Atmos. Chem. Phys. Discuss.* **15**, 16111–16139 (2015). <https://doi.org/10.5194/acpd-15-16111-2015>
- Yadav, R.R., Park, W.K., Singh, J., Dubey, B.: Do the western Himalayas defy global warming? *Geophys. Res. Lett.* **31** (2004). <https://doi.org/10.1029/2004GL020201>

Publisher's Note Springer Nature remains neutral with regard to jurisdictional claims in published maps and institutional affiliations.

Springer Nature or its licensor (e.g. a society or other partner) holds exclusive rights to this article under a publishing agreement with the author(s) or other rightsholder(s); author self-archiving of the accepted manuscript version of this article is solely governed by the terms of such publishing agreement and applicable law.